RSC Advances

ROYAL SOCIETY OF CHEMISTRY

www.rsc.org/advances

Journal Name

ARTICLE TYPE

Cite this: DOI: 10.1039/xxxxxxxxxx

Systematic study on the impact of water on the performance and stability of perovskite solar cells†

Charlotte Clegg, and Ian G. Hill

Received Date
Accepted Date

DOI: 10.1039/xxxxxxxxxx

www.rsc.org/journalname

The effects of water on the photovoltaic performance of methylammonium lead iodide perovskite devices has recently become a topic of interest within the perovskite community. However, existing studies report contrasting and sometimes contradictory observations. In this work, small concentrations of water, consistent with those present in air-exposed DMF, were systematically incorporated directly into the PbI_2 precursor solution in order to investigate its effect on the performance of sequentially spin-coated, inverted perovskite solar cells. Increasing concentrations of water in the PbI_2 solution were found to have a negative impact on photovoltaic performance. The addition of water was observed to exaggerate the scan-rate and directional-dependent hysteresis and introduce new transient behaviours in comparison to the "dry" devices. Interestingly, the addition of water was also found to improve the long-term device stability in comparison with devices fabricated from "dry" precursors.

1 Introduction

Perovskite photovoltaics have rapidly risen to the forefront of next generation photovoltaic technologies. In just over five years, the power conversion efficiencies of methylammonium lead halide perovskites have improved from a modest 3 %, to a certified 20.1 %.[1,2] The increased performance is owed largely to improvements in device architecture, film coverage and morphology. However, several unique properties, such as low exciton binding energies, low charge carrier recombination rates (and long carrier diffusion lengths) and the ability to absorb strongly across the visible spectrum, have made these materials promising candidates for next generation solar cells.[3–6] Many groups have shown that high device efficiencies can be achieved using relatively simple low-temperature solution processing techniques, which can easily be applied to large-scale roll-to-roll manufacturing processes.[7–13] Slot-die coated and inkjet printed perovskite devices have already achieved efficiencies in excess of 10 %, a promising indicator for the commercial viability of this technology.[14,15]

Despite such remarkable successes, perovskite photovoltaics are not without shortcoming. Methylammonium lead iodide perovskites are known to be extremely sensitive to water. Still, there is disagreement in the literature regarding the severity and reversibilty of water-induced degradation; and the exact degradation pathway(s) through which water interacts with the perovskite bulk remains unclear.[16–20,22?,23] Yang et al. systematically documented the degradation rates of perovskite films in controlled humidity environments via the formation of a hydrated intermediate.[18] The degradation process was found to be at least partially reversible, which is similar to observations by Leguy et al., who documented the formation of a monohydrate perovskite phase upon exposure to a humid environment.[19] Leguy et al. found that the hydrated perovskite demonstrated, approximately, a 90 % reduction in the short circuit current density and 0.2 V decrease in the open circuit voltage; surprisingly, the authors reported complete reversibility after exposure to dry nitrogen for four hours. Conversely, Zhou et al. reported that a water vapour spray treatment of perovskite films resulted in improved crystallinity; the effect was found to be similarly reversible.[24] Through similar investigations, many authors have shown that exposure to ambient water vapour is less detrimental to perovskites than previously thought. Indeed, exposure to ambient moisture during the precursor, deposition, annealing or post-fabrication stages can result in significant enhancements to the final device performance.[25–29]

Despite the growing interest in this new topic, several conflicting reports exist in the literature. Using a sequential spin coating procedure, Wu et al. report a dramatic improvement in the morphology of neat PbI_2 films with the addition of 2 wt% H_2O to the precursor solution. Their optimized fabrication procedure yielded an 18 % efficient device in comparison with their control device, which achieved a maximum power conversion effi-

Dalhousie University, Department of Physics and Atmospheric Science, 6310 Coburg Rd., Halifax, Canada. Fax: 902-494-5191; Tel: 902-494-3897; E-mail: ian.hill@dal.ca

† Electronic Supplementary Information (ESI) available: tables, statistical summaries of performance metrics, transient photocurrent fits and SEM images for devices/films fabricated with varying concentrations of H_2O in the PbI_2 film. See DOI: 10.1039/b000000x/

ciency of 0.0063 % using an anhydrous solution of PbI_2.[30] Also using a sequential deposition procedure, Adhikari et al. note that an optimized device performance and charge carrier lifetime are achieved with a concentration of 5 vol% H_2O in the methylammonium iodide dipping solution.[31] Conings et al. performed a similar study using a well documented mixed halide, single-step deposition procedure. They observed little overall change in device performance with the substitution of up to 10 vol% of the anhydrous DMF solvent with deionized H_2O, suggesting that the required fabrication environment may be more flexible than previously thought.[32] In contrast, Gong et al. report an enhancement in both photovoltaic performance and stability with the addition of 2 vol% H_2O to the same single-step precursor solution.[33] Such a wide variation in observations suggests that the effects of water on the morphology and performance of methylammonium lead halide devices are still not well understood; and, that more work is needed in order to elucidate the precise mechanism(s) through which water interacts with this unique material.

In this study, the effects of moisture on the photovoltaic performance and properties of perovskite devices were examined under highly controlled fabrication conditions. To minimize uncontrolled exposure to moisture, synthesis and testing of perovskite devices were all carried out in a dry, argon filled glovebox, save for the addition of controlled volumes of de-ionized, water to the PbI_2 solutions. It is well known that the morphology of the perovskite layer plays a critical role in the final device performance.[34–36] Pinholes and film dewetting not only result in decreased absorbance by the perovskite layer, but also a greater number of recombination pathways (and consequently poorer device performance); therefore, the perovskite films in this study were fabricated via sequential spin-coating to reduce any effects that the contrasting solubility of the lead iodide (PbI_2) and methylammonium iodide (MAI) precursors in water may have on film homogeneity.[28]

2 Experimental methods

2.1 Perovskite fabrication methods

2.1.1 Solution preparation.

All solvents, MAI (Dyesol, $\geq$ 98%) and PbI_2 (Alfa Aesar, 99.9985 %) were opened and stored under argon. To avoid inadvertent exposure to moisture, all vials and stir bars were baked at $\sim$120 ^oC in the argon filled glovebox prior to use. MAI was mixed with anhydrous isopropanol (Aldrich, 99.5 %) to form a dry 47.5 mg/mL stock solution. A 450 mg/mL dry lead iodide solution was mixed by stirring the measured PbI_2 with anhydrous DMF (Aldrich, 99.5 %) at 70 ^oC. A 30 mg/mL solution of phenyl-C_{61}-butyric-acid-methyl ester (PCBM, Solenne, $\geq$ 99.5%) was mixed in chlorobenzene, also at 70 ^oC. The PbI_2 and PCBM solutions were stirred at 70 ^oC for at least 12 hours prior to use, and were maintained at 70 ^oC throughout the fabrication process. Water concentration in the "wet" solutions was varied as: 0, 1, 2, 4 and 6 mol % with respect to the solute (i.e. mol % = $[H_2O]/[PbI_2]$ x 100, where $[PbI_2]$ = 0.976 M). Although this is up to two orders of magnitude lower than the concentrations used by other authors, it was identified as a region of interest based on the amount of water measured to have been absorbed by a DMF-based solution at 50 % relative humidity after 20 minutes (0.025 mol/L, which translates to $\sim$2.6 mol% with respect to 450 mg/mL of PbI_2).[37,38] Therefore, this represents the range of water concentrations that would be expected to be inadvertently incorporated into precursor solutions due to air-exposure during fabrication in an ambient environment. "Wet" PbI_2 solutions were made by mixing the solute with appropriate ratios of dry solvent and "wet" solvent (a 10 μL/mL mixture of de-ionized H_2O in the dry solvent). The "wet" solvent was mixed and added to the PbI_2 solution 8 hours prior to fabrication in order to minimize the extent to which DMF may be hydrolyzed into formic acid and dimethylamine, while also ensuring dissolution of the PbI_2, which is poorly soluble in water.[39] Because water has a significant vapour pressure at 70 ^oC, the volumes of the "wet" PbI_2 solutions were mixed to minimize head space in the vial and consequent water loss from the heated solution. Such measures were found to be critical when dealing with low concentrations of water; assuming a head space of 2 mL (in a standard 4 mL glass vial), the expected partial pressure of water at 70 ^oC corresponds to $\sim 2.19 \times 10^{-5}$ mol of H_2O in the vapour phase. This amounts to nearly 20 % of the added water in 2 mL of a PbI_2 solution with 6 mol% water and over 100 % of the added water in 2 mL of a solution with 1 mol% water. All solutions were passed through 0.45 μm filters into clean glass vials prior to use in order to avoid including unwanted particles in the final films. The solutions were recapped immediately to avoid water loss. Although it is impossible to be certain of the precise fabrication details used by other authors, it is possible that the reported water concentrations in the perovskite precursor solution may be a source of discrepancy in existing literature. However, rigorous measures were taken in this study to ensure that the quantities of water incorporated into the precursor solutions were as well-defined as possible.

2.1.2 Device fabrication.

ITO substrates (2.5 x 2.5 cm) were patterned using a Kapton tape mask and etched in a 12 M HCl bath. Substrates were scrubbed with detergent and de-ionized (DI) water, then ultrasonicated in baths of detergent, DI water, acetone and ethanol for 20 minutes each. Finally, substrates were treated with UV-ozone for 20 minutes. The PEDOT:PSS layer was formed by casting 90 μL of a filtered stock of Clevious AI 4083 onto each ITO substrate and spinning at 3000 rpm in air for 60 s. The films were annealed at 140 ^oC for 60 minutes, then rapidly transferred into an argon filled glovebox for the remainder of the fabrication procedure. 300 μL of 70 ^oC PbI_2 solution was cast onto the cooled PEDOT:PSS and spun at 6000 rpm for 180 seconds, then 8000 rpm for 180 seconds. Completed films were dried on a 70 ^oC hotplate for 15 minutes. The perovskite was formed by casting 400 μL of MAI solution onto the lead iodide film, spinning at 6000 rpm for 150 seconds, then annealing at 100 ^oC for 2 hours. 150 μL of 70 ^oC PCBM solution was cast onto the cooled perovskite films, spinning at 1000 rpm for 180 seconds, then annealing at 100 ^oC for 45 minutes. The devices were completed by thermally depositing 15 nm of calcium and 100 nm of aluminium (at $\sim 10^{-6}$ Torr) as a top contact. (The thicknesses of the PEDOT:PSS, perovskite and

PCBM layers for these devices were estimated to be 50 nm, 270 nm and 80 nm, respectively, using a Dektak profilometer). The area of the completed devices was defined by the overlap between the top contact and the ITO strip, which was 0.035 cm^2. Finally, to minimize any effects due to batch-to-batch variations, devices of all five H_2O concentrations were fabricated on the same day using the same PEDOT, MAI and PCBM stock solutions, with the top contacts deposited on all five substrates simultaneously.

2.1.3 Film fabrication.

All characterization (XRD, SEM, UV-vis absorption and steady state photoluminescence measurements) was performed on perovskite films, which (unless otherwise stated) were made concurrently with devices. Glass slides (2.5 x 2.5 cm) were cleaned in the same manner as the ITO substrates, then coated with PEDOT:PSS and the perovskite as specified in the previous section. The completed films were stored in the glovebox until the characterization measurements were performed.

2.2 Device characterization

Current density-voltage (JV) data were measured under simulated AM1.5G sunlight at 100 mW/cm^2 using a ScienceTech solar simulator and a Keithley 236 source measure unit. The illumination intensity was calibrated using a calibrated silicon photodiode/KG5 glass filter combination. JV data were collected by sweeping from 1.5 V to -1.0 V (reverse scan) and -1.0 V to 1.5 V (forward scan) using two scanning rates: 1.0 V/s and 0.1 V/s. Transient photocurrent measurements were performed by holding the device at 1.5 V for 2 seconds, then measuring the short circuit current density as a function of time for up to 500 seconds.

2.3 Film characterization

Optical absorption measurements were collected with a Cary UV-vis spectrophotometer using a 300 nm/min scan rate. Steady state photoluminescence (PL) measurements were collected using a Cary Eclipse spectrophotometer; an excitation wavelength of 520 nm and 120 nm/mim scan rate were used. A Phenom benchtop SEM was used to obtain scanning electron microscopy images of the perovskite films. A Siemens D5000 x-ray diffractometer was used to obtain structural information about the films. Patterns were collected by sweeping from a scattering angle of 2θ = 10° - 60° in 0.05° steps with a 5s/step dwell time. The divergence, anti-scattering and receiving slits were 0.5°, 0.5°, and 0.1 mm, respectively. Separate films were fabricated for the XRD measurements to prevent degradation effects due to extended exposure to high energy x-ray irradiation in an ambient environment. Unless otherwise specified, all characterizations were performed in an ambient atmosphere, on glove-box stored films, within 24 hours of measuring the associated device (JV) performance.

3 Results and discussion

3.1 Device performance

Figure 1 compares the best devices achieved using varying concentrations of H_2O in the PbI_2 solution. A dramatic decrease in

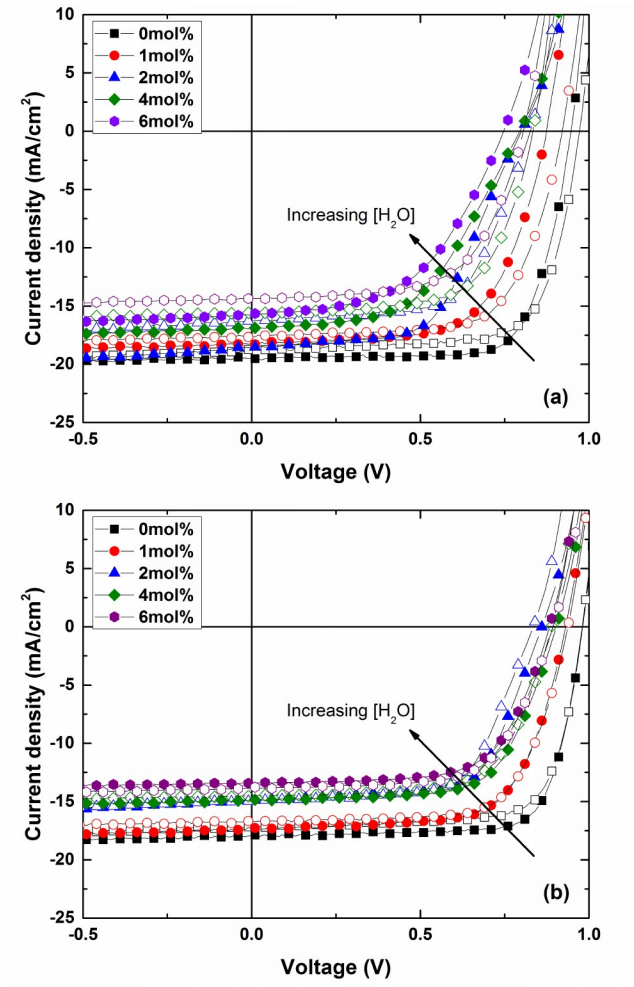

Fig. 1 JV curves of the best performing cells for devices made using varying concentrations of H_2O in the PbI_2 solution measured with (a) a 1.0 V/s scan rate, and (b) a 0.1 V/s scan rate. Reverse sweeps are indicated by the shaded symbols, while forward sweeps are indicated by the unshaded symbols.

device performance is observed when increasing concentrations of water are added to the PbI_2 precursor solution: the addition of 1 mol% of H_2O results in a decreased open circuit voltage, by ~ 100 mV, which is also accompanied by a minimum 10% decrease in the device fill factor. The loss of open circuit voltage and fill factor continues when the concentration of water in the PbI_2 solution is further increased. When the water content is increased beyond 2 mol%, a drop in photocurrent, by up to ~ 4mA/cm^{-2} is also observed. Together, these three trends have severely detrimental effects on overall device performance, as illustrated in Figure 2. (A full tabulation of the average and best device performances under different scan rates is available in ESI Tables 1 – 2†).

These trends are contrary to existing reports, where the addition of water is seen to either: yield a peak device performance using a specific concentration of water (Wu et al. and Gong et al.);[30,33] or, produce no observable effect on morphology and overall device performance (Conings et al.).[32] Conings et al. do note a similarly sustained drop in open circuit voltage with the addition of water to the perovskite precursor, but the ef-

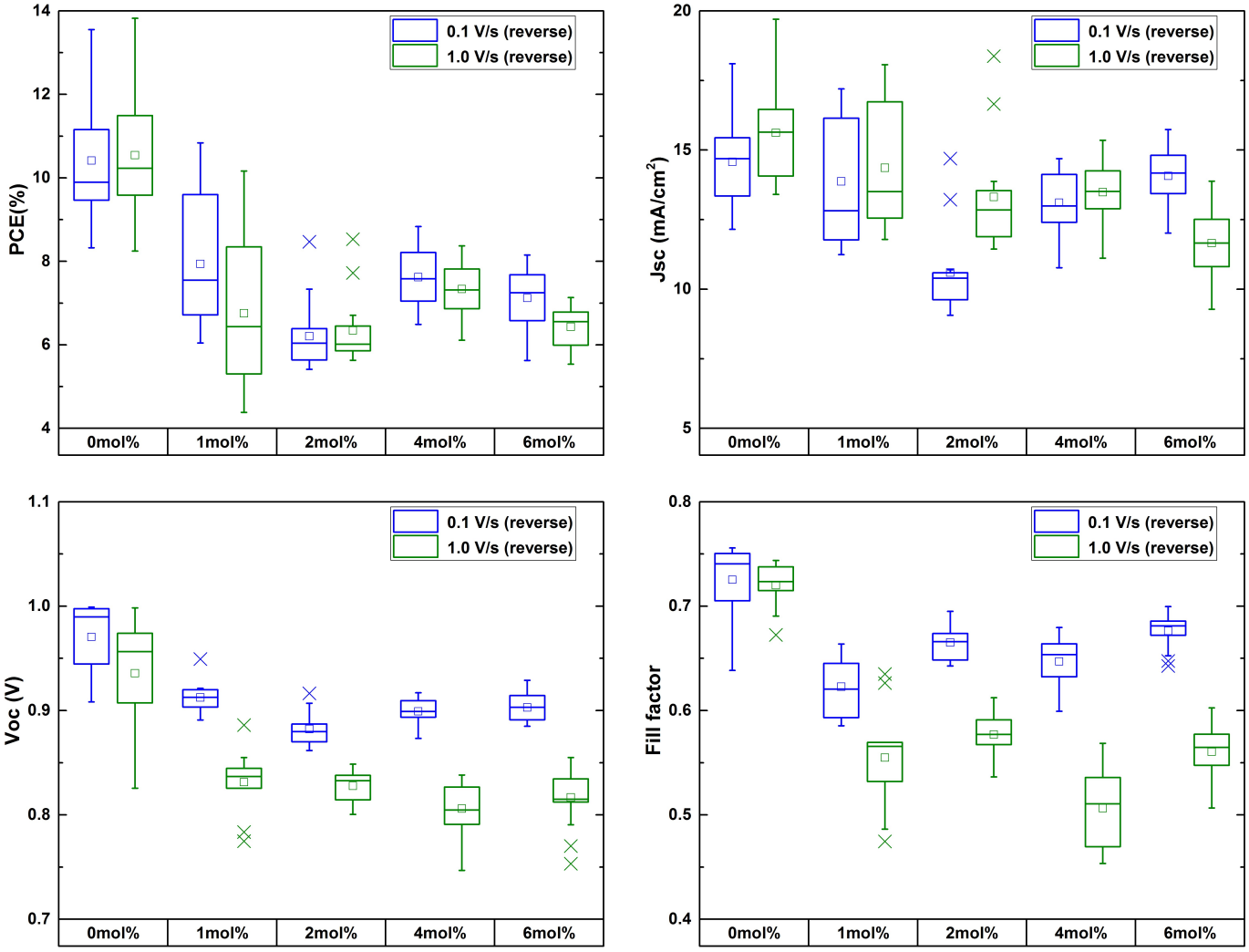

Fig. 2 Summary of performance metrics for devices made using varying concentrations of H_2O in the PbI_2 solution. Data are representative of 9 - 16 devices tested by sweeping in the reverse direction at 0.1 V/s (blue) and 1.0 V/s (green). The spread of the data, mean, median and outliers are represented by the vertical bars, small square, horizontal line and crosses, respectively.

fect is compensated by an increase in photocurrent, resulting in no change in the overall device performance. The variety of observations are difficult to resolve; however, the reported device fabrication procedures differ between each of existing studies as well from the methods used in this study. As well, the added water may interact differently when used in different perovskite precursors (i.e: single-step mixed halide solution in comparison to sequential spincoating of the two perovskite precursors). Currently, the only other studies to examine the impact of added water to sequentially spin coated perovskite devices are less well-controlled, with all fabrication being performed in ambient conditions, where atmospheric water vapour may also contribute to the observed trends.[30,31] We also highlight the superior performance of our control devices, and the fact that we have chosen to investigate the addition of much smaller volumes of water, with the belief that such volumes of water are more representative of those which may be inadvertently incorporated into the precursor during fabrication in air.

With respect to the anomalous hysteresis, which has been well-documented by many authors,[40–43] very little was observed when the devices were measured using a 0.1 V/s scan rate. The JV data from the forward and reverse sweeps in Figure 1 are nearly identical. This is further illustrated in Figure S1†, which summarizes the batch statistics for several devices made using the same fabrication conditions; the difference between the reverse and forward scans is most reflected by a decreased open circuit voltage (up to $\sim$ 400 mV decrease) for devices with water added to the PbI_2 solution. Scanning at 1.0 V/s, resulted in a greater amount of hysteresis (Figures 1 and S2†), which was exaggerated by further addition of H_2O to the PbI_2 solution. The lack of appreciable hysteresis in these devices is not surprising given that reduced hysteresis is often reported in inverted architecture perovskite devices.[7,10,12,30,44,45] It has been suggested that the level of hysteresis is heavily influenced by particular charge selective

contacts,[45,46] where PCBM is additionally thought to passivate trap states within the perovskite that contribute to photocurrent hysteresis.[47,48]

To further examine device hysteresis, the temporary enhancement by forward biasing (TEBBing, documented by O'Regan et al.) and its effect on the measured current density were measured.[42] Each device was held at +1.5 V bias under 1 sun illumination for 2 seconds before measuring the short circuit current density over 20 seconds. Although strong evidence has been shown to suggest that bias history, and not light soaking, is responsible for hysteresis,[42,43] each device was held at zero bias in the dark for 1 minute prior to measurement to minimize any possible contributions from competing light-driven effects, which have been suggested by other authors.[40,49] The transient photocurrents measured over the 20 second period are shown in Figure 3 (a), normalized to their initial photocurrent (at t = 0 seconds). Interestingly, opposite dynamics were observed for devices made using dry precursors and devices made using "wet" precursors. The devices measured with no moisture added to the PbI_2 solution exhibit a photocurrent decay. In contrast, all devices fabricated with added water experience a growth in photocurrent, which extends beyond the 20 second measurement period. As observed by other authors, the transient behaviour for each device is observed to be strongly biexponential;[42,50] the time constants extracted from a biexponential fit to each of the transient behaviours are shown in Figure 3 (b). The slow time components of the photocurrent growth at 0 V are similar in magnitude to those reported by Eames et al. after holding a device in the dark at -0.5V for 100 seconds. In this study, the magnitude of the time constants are seen to increase gradually with the included moisture content of the devices (Figure 3 (b)). An anomaly is observed in devices made using 2 mol% H_2O in the PbI_2 solution, which demonstrate an initial photocurrent decay, followed by monoexponential growth. Such behaviour suggests that two competing transport mechanisms may coexist within perovskite films.

The transient photocurrent measurements were repeated over a 500 second time scale, shown in Figure 4. The reverse, then forward JV sweeps of the corresponding devices were also measured at various scan rates (1.0 V/s, 0.1 V/s, then 0.01 V/s). Again, devices fabricated from a dry PbI_2 solution were seen to exhibit a photocurrent decay; whereas, devices fabricated from "hydrated" precursors demonstrated a photocurrent growth with time. The steady state photocurrent observed in Figure 4 (a) nearly converges with the JV photocurrent measured from the same device at the slowest scan rate. As indicated by other authors this suggests that only very slow JV sweep rates ($\leq$0.01 V/s) are truly reflective of steady state device operation.[40] Unexpectedly, the transient photocurrent growth observed in "hydrated" devices is not accompanied by an increased photocurrent at slower scan rates, but rather a decreased photocurrent and an increased open circuit voltage.

Transient behaviours and anomalous hysteresis are commonly suggested to result from the motion of ionic species within the perovskite layer: I^-, MA^+ and Pb^{2+}.[41,43,47,50–53] Although the suggested activation energy and migration time scale for each

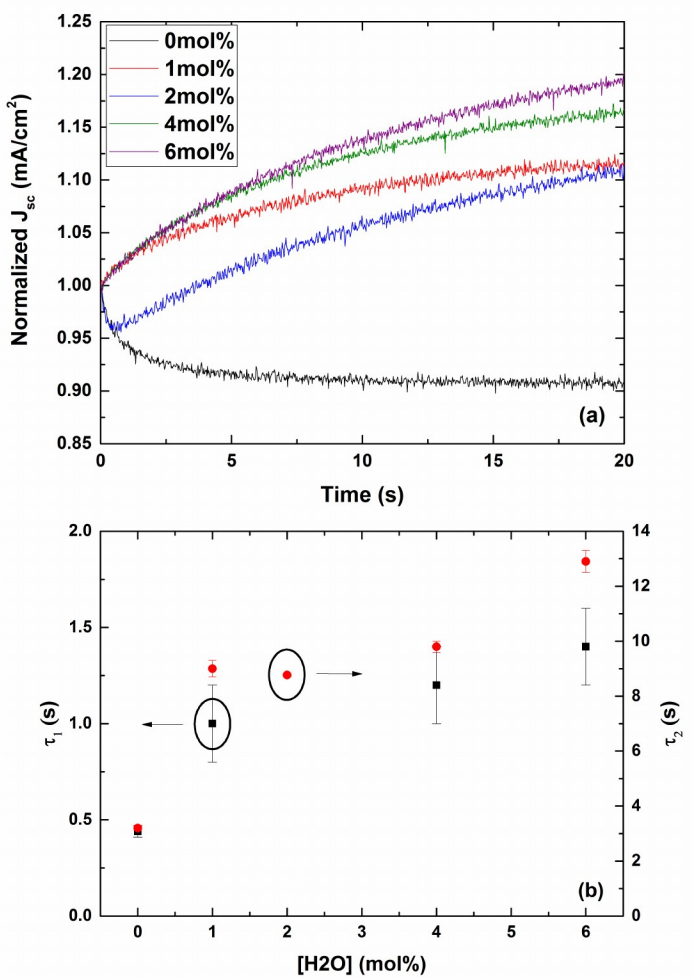

Fig. 3 Representative transient photocurrent behaviours for devices with varying concentrations of H_2O in the PbI_2 solution, (a). The time constants extracted from a biexponential fit of each curve are shown in (b), where τ_1 is shown on the left axis in black, and τ_2 is shown on the right axis in red. The anomalous behaviour of the 2 mol% device was treated by applying a single exponential fit to the transient growth to extract the second time constant.

species varies between studies, I^- consistently appears to exhibit the highest mobility, followed by MA^+ and Pb^{2+}.[22,50–52] Shao et al. have also produced convincing experimental evidence linking I^- migration with hysteresis.[53]

In the presence of water, H_2O incorporation into the perovskite is thought to be energetically favourable, leading to its spontaneous infiltration into the lattice.[22?] Both computational and experimental studies suggest that the absorbed water interacts strongly with the methylammonium cation and surrounding iodine atoms through hydrogen-bonding;[22?] however, the ultimate degradation pathway(s) caused by water exposure are not agreed upon. Some authors propose an acid-base reaction, whereby a single water molecule may be sufficient to degrade the material, but an excess of water is required to dissolve the byproducts.[16,54]

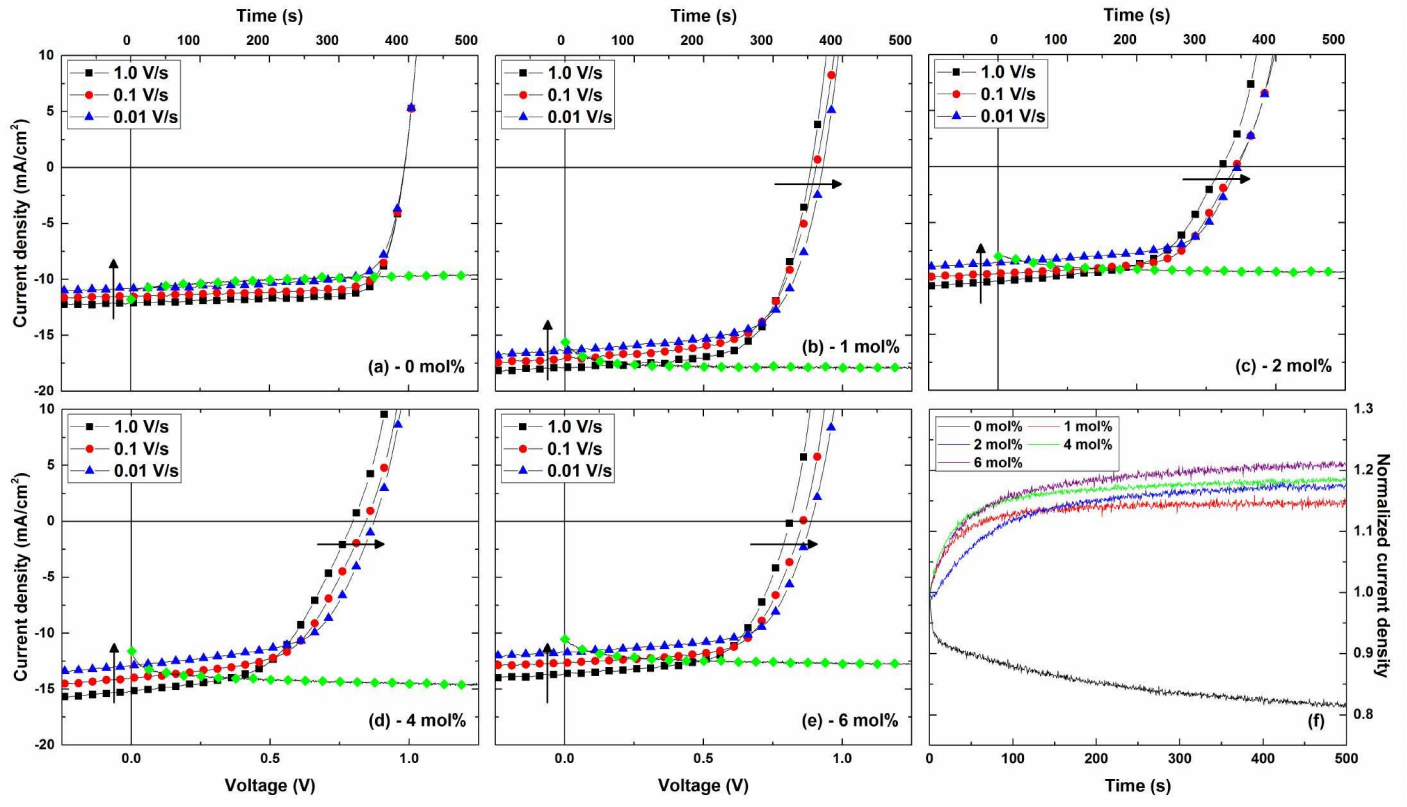

Fig. 4 Rate dependent JV measurements (for reverse sweeps) and transient photocurrent behaviours for the corresponding devices with varying concentrations of H_2O in the PbI_2 solution, (a) - (e). The transient photocurrents are plotted in green, and correspond to the time axis from 0 to 500 seconds. The transients shown in (a) - (e) are contrasted in (f), normalized to the initial photocurrents. (The measurements shown in this figure were taken 20 days post-fabrication. Results from a biexponential fit to each transient photocurrent are summarized in the ESI†.)

$$n[(CH_3NH_3^+)PbI_3] + H_2O \longrightarrow$$
$$[(CH_3NH_3^+)_{n-1}(CH_3NH_2)nPbI_3][H_3O] \longrightarrow \quad (1)$$
$$HI + CH_3NH_2 + H_2O + PbI_2 + (n-1)[(CH_3NH_3^+)PbI_3]$$

Other authors suggest a reversible hydration of the perovskite, where irreversible degradation is only achieved if an excess of water is present to dissolve the $CH_3NH_3^+$.[18,19]

$$4(CH_3NH_3)PbI_3 + 4H_2O \rightleftharpoons 4[CH_3NH_3PbI_3 \cdot H_2O] \rightleftharpoons$$
$$(CH_3NH_3)_4PbI_6 \cdot 2H_2O + 3PbI_2 + 2H_2O \quad (2)$$

Regardless of the exact degradation pathway, the addition of water in this study likely increased the population of mobile ions within the perovskite film, and may have changed the activation energy associated with the migration of each species. A larger number of mobile ionic species would explain the increased hysteresis observed when higher concentrations of water were included in the perovskite film. For the "dry" perovskite, the I^- ions would migrate towards the device anode under the two-second forward bias treatment. Assuming that the transport of such species is restricted to motion within the perovskite layer, extended forward biasing would cause an accumulation of negative charge near the PEDOT/perovskite interface. This in turn would create an internal electric field, which would facilitate hole extraction. Once the device is short-circuited, the build-up of I^- ions would be driven by a concentration gradient to diffuse away from the interface, resulting in a decreased charge collection efficiency over time and hence a decreased photocurrent (Figure 4). This behaviour is also reflected in the sequence of JV sweeps presented in Figure 4; reverse sweeps performed at slower scan rates would allow greater relaxation of the ionic concentration gradient, resulting in a decreased charge collection efficiency and, therefore, a lower photocurrent.

It is speculated that the addition of water may favour the motion of MA^+ over I^- ions. In pure monohydrate and dihydrate perovskite crystals, water is incorporated between the $[PbI_6]^{4-}$ octahedra with the methylammonium cation, resulting in an arrangement of $[PbI_6]^{4-}$ octahedra separated by methylammonium ions and H_2O.[19,23,55] Although no crystalline hydrate phases were observed in this study within the detection limits of XRD (Figure 6), it is possible that sufficient water was incorporated into the perovskite lattice to disrupt the caging of the MA^+ cation, and facilitate its migration through the film. Other authors have also suggested that the methylammonium cation is deprotonated in the presence of H_2O,[16,54] which could allow liberated H^+ ions to mi-

grate through the lattice and contribute to the transient photocurrent. The energy barrier for H^+ migration is suggested to be lower than that for intrinsic ionic species such as $CH_3NH_3^+$ and I^-.[50,56] This difference in energy barriers could account for the difference in transient dynamics observed between "dry" and "hydrated" devices. Under the two-second forward bias treatment, the mobile MA^+ (and possibly H^+) ions would migrate towards the device cathode, resulting in an accumulation of positive charge at the perovskite/PCBM interface. The accumulation of positive charge would create a localized potential well, trapping electrons and therefore decreasing the measured photocurrent. Once the device is short-circuited, the MA^+ ions would diffuse away from the interface, allowing for more efficient charge collection over time. This behaviour is also reflected in the sequence of JV sweeps presented in Figure 4 when considering the entire biasing history of the device. After the reverse sweep (+1.5V to -1.0V) at 1.0 V/s, the device is immediately scanned in the forward direction (-1.0V to +1.5V) before it is again measured in the reverse direction (+1.5V to -1.0V) at 0.1 V/s. Therefore, the most recent biasing history of the device before the reverse sweep at 0.1 V/s is 1.5 seconds at increasing forward bias, which results in positive ion accumulation at the perovskite/PCBM interface. The effect would be exaggerated for progressively slower scan rates; thus, the slowest scan rate (which was previously forward biased for the longest amount of time) should experience the largest photocurrent suppression. Although the suggested model of ion migration agrees well with experimental data, a more detailed investigation is necessary to verify these postulates and is currently underway.

3.2 Effect of water content on film morphology:

Figure 5 shows a series of top view SEM images for perovskite films fabricated with varying concentrations of water in the PbI_2 solution and a dry (0 mol% H_2O) MAI solution. In order, the images show perovskite films fabricated with 0 mol%, 1 mol%, 2 mol%, 4 mol% and 6 mol% H_2O in the PbI_2 solutions, respectively. The final image is of a PbI_2 film with 0 mol% H_2O, illustrating the high surface coverage of the PbI_2 layer. Overall, the perovskite films appear to exhibit a compact, dense morphology and a high surface coverage. Films fabricated with less than 4 mol% H_2O in the PbI_2 solution exhibit higher surface coverage, with the majority of the grain sizes falling below 200 nm, and a small fraction of grains exceeding 500 nm in size. In contrast, a much higher fraction of grains are larger than 500 nm in films fabricated with 4 mol% and 6 mol% H_2O in the PbI_2 solutions, with some grains sizes even appearing to exceed 1 μm. These films, however, show a lower surface coverage with a significantly increased density of pinholes and cracking between larger grains. (Details are available in the ESI†). Similar trends regarding increased grain size and pinhole formation have also been reported in other studies where moisture is introduced during the perovskite fabrication procedure.[26–29,32,33]

The observed trends in film morphology are congruent with trends observed in device performance. The increased cracking and pinhole formation in films with more moisture introduce a greater number of shunt pathways, which could explain the reduction in short circuit current and open circuit voltage for devices made with higher concentrations of water (Figures 1 and 2). It is also possible that larger perovskite grain sizes could be accompanied by increased film roughening in the z-direction, leading to incomplete coverage by the PCBM layer and therefore greater recombination at the interface between the perovskite and the top contact.

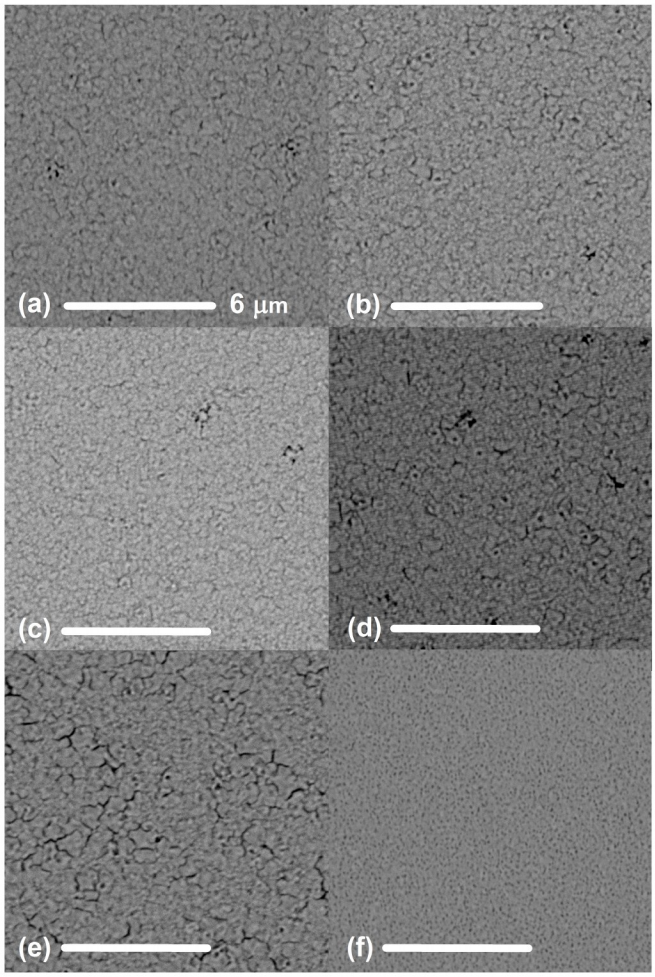

Fig. 5 Top view SEM images of films made with varying concentrations of H_2O in the PbI_2 solution: (a) 0 mol%, (b) 1 mol%, (c) 2 mol%, (d) 4 mol% and (e) 6 mol%. A film of unconverted PbI_2 with 0 mol% H_2O is shown in (f). The scale bar represents 6 μm. Images were taken in regions corresponding to the device locations on the substrate. (Details are available in the ESI†).

Figure 6 shows a series of XRD patterns for films made with varying concentrations of H_2O in the PbI_2 solutions. The patterns indicate that the tetragonal (*I4cm*) $MAPbI_3$ perovskite phase was successfully formed in all instances with strong preferential orientation in the (110) direction, as is typical of spin coated $MAPbI_3$ thin films. All films are also seen to exhibit similar relative peak intensities. Interestingly, perovskite films fabricated with low concentrations of H_2O in the PbI_2 solution (0 mol% and 1 mol%) contain detectable amounts of crystalline PbI_2, while the other films do not. Gangishetty et al., also observed incomplete conversion and residual crystalline PbI_2 when sequential-step perovskite

conversion was carried out in a low humidity environment (RH = 1%), while conversion under higher relative humidity was observed to yield phase pure perovskite.[29] Whether the presence of the residual PbI_2 peaks observed in this study is due to degradation during the annealing process, or simply due to incomplete conversion is unknown. As suggested by Gangishetty et al, it is possible that the presence of moisture may facilitate MAI incorporation into the PbI_2/perovskite lattice by favouring the presence of a less-compact intermediate hydrate phase. It is also interesting to note that the higher performance of the 0 mol% and 1 mol% H_2O devices corresponds to films with residual PbI_2, which is consistent with the passivating effects of lead iodide suggested by other authors.[57,58] Although these hypothesis are well-supported by the presented data (Figures 5 and 6), it is important that the presence (or absence) of crystalline PbI_2 in Figure 6 (a) be regarded with caution due to the inherent limitations of using the Bragg-Brentano diffraction geometry to indicate phase composition within a thin-film sample.

In this study, no significant enhancement in the diffraction intensity is observed with increasing moisture in the PbI_2 solution. The fact that other studies have observed increased device performance and crystallinity in perovskite films that were annealed under high relative humidity suggests that the use of ambient moisture may act as a means of solvent vapour annealing.[26] It is interesting to note that very similar effects to those reported in published moisture studies (that examine the effects of annealing treatments under controlled humidity environments) have also been observed in perovskite films treated with DMF solvent vapour.[59] It therefore seems possible that the photophysical enhancements observed in such published reports may primarily be a consequence of morphological changes rather than any chemical changes resulting from the incorporation of water into the perovskite lattice.

Finally, although the Debye-Scherrer equation is typically only valid when analysing very small crystal sizes (< 50 nm), the slight broadening of the (110) perovskite peak for films made with drier PbI_2 (Figure 6 (b)) may be correlated with the higher proportion of smaller crystal sizes observed within the bulk of the "drier" perovskite films. The absence of unidentified peaks or diffraction signals at ~ 8.7, 11.6 or 11.7° also suggests that any effects from impurities and hydrated intermediates, or precursors can be excluded in our consideration of the observed trends in this study.[18,19,60]

3.3 Photophysics of the perovskite devices

Figure 7 demonstrates the UV-vis absorption and photoluminescence spectra for perovskite films made with varying concentrations of H_2O in the PbI_2 solution. All of the films can be seen to exhibit similar absorption spectra, with no appreciable contribution from any residual lead iodide. The film made with no added water exhibits a nominally higher absorbance than the other films. In general, the absorption intensity of films is seen to decrease with increasing concentrations of water. However, it is difficult to ascertain whether this observation is a real trend, or merely a chance effect resulting from variations in scattered

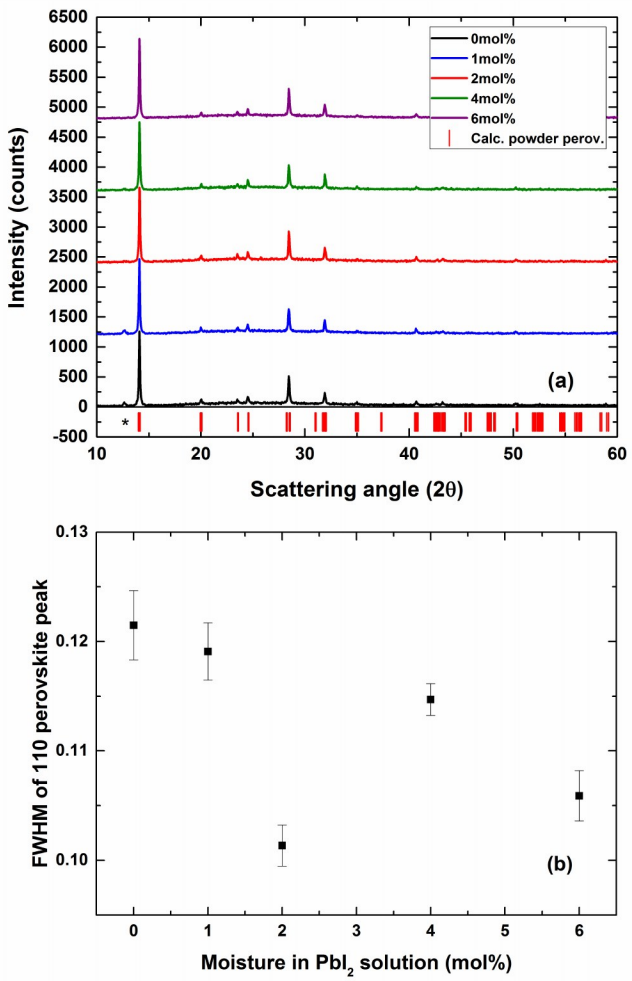

Fig. 6 Unnormalized XRD patterns of films with varying concentrations of H_2O in the PbI_2 solution, (a). The red ticks indicate the calculated powder perovskite diffraction pattern of the tetragonal *I4cm* phase; while, the black asterisk marks the location of the (001) PbI_2 diffraction peak. Patterns are offset by 1200 counts for clarity. The FWHM of the (110) perovskite peak is plotted as a function of H_2O concentration, (b).

light between samples, or light transmission through cracks or pinholes. The characteristic perovskite PL emission is observed at ~789 nm, with the highest intensity emission corresponding to the perovskite film made using dry precursor solutions. The intensity of the photoluminescent peak can be seen, generally, to decrease with the increasing addition of water to the lead precursor solution. This trend suggests an increased number of non-radiative recombination pathways, possibly due to an increased number of deep trap states, which would not be passivated by the PCBM layer.[47,48] This is consistent with the decreased device performance observed in perovskite films with added moisture (Figure 1). Leguy et al. link a decrease in device performance with the appearance of a hydrate phase after exposure to 77 % relative humidity for 3 hours.[19] Although no crystalline hydrate phase is observed in this study (Figure 6), it is possible that the inclusion of water in the PbI_2 precursor may have resulted in small quantities of a hydrated-perovskite phase dispersed throughout the film, which would act as recombination centres for photo-

generated charge. Finally, peak fitting of the photoluminescent spectra reveals a slight blue shift ($\Delta\lambda = \sim 3$ nm) in the peak luminescence wavelength with the addition of increasing quantities of water (Figure 7 (b), inset). Similar trends have been observed by other authors, where exposure of the perovskite to water is linked with a blueshifted PL spectrum.[24,61] The observed blueshift is suggested to arise from lattice strain as water is incorporated into the perovskite crystal.[22,61]

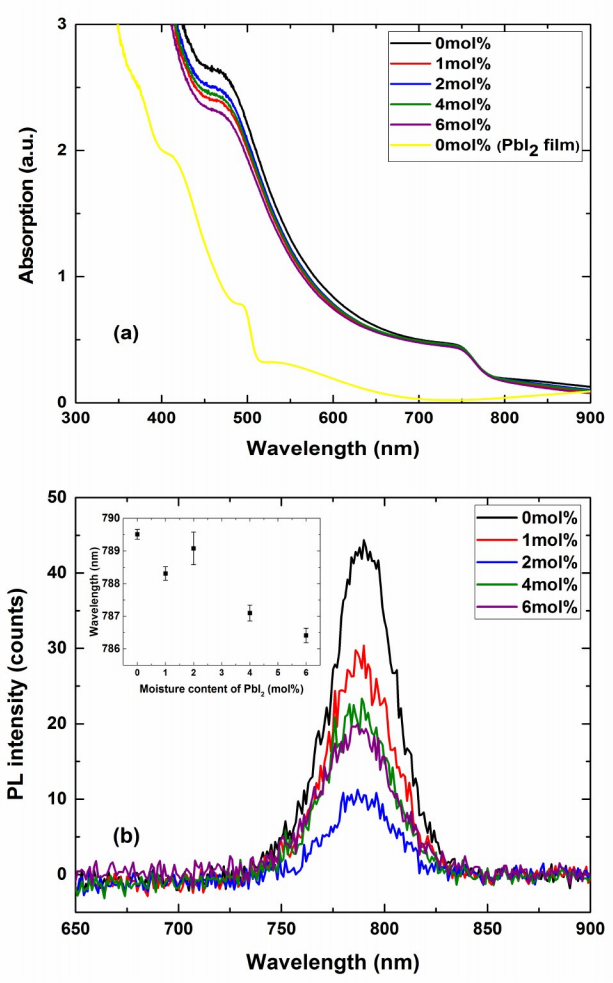

Fig. 7 (a) UV-vis absorption and (b) photoluminescense spectra of films made with varying concentrations of H_2O in the PbI_2 solution, measured within 24 hours of device testing.

3.4 Effect of moisture content on device stability:

Remarkably, the inclusion of moisture into the perovskite layer via the PbI_2 precursor is observed to have a stabilizing effect on device performance over time. Figure 8 compares the JV curves for devices tested within 24 hours of fabrication with devices tested 20 days post-fabrication. The performance metrics are summarized in Table 1. All devices were stored under argon, and were at no point exposed to an ambient atmosphere. The best anhydrous device was observed to experience, roughly, a 25 % decrease in power conversion efficiency and 30 % decrease in photocurrent after 20 days storage under argon. The severity of the performance loss is alleviated by the inclusion of water in the PbI_2 solution, with the best 1 mol% yielding the greatest stability and a higher PCE than the best dry device after 20 days. Only a 9 % decrease in the measured power conversion efficiency was observed in the 1 mol% device after 20 days. Wu et al. and Gong et al. both report good device stabilities for their optimized devices in comparison to their control device, noting only a 10 % and 8 % reduction in PCE after 40 and 6 days, respectively.[30,33] As far as we know, however, this is the first report where long-term device stability under inert conditions is explicitly linked to all devices with included moisture. In the context of this study, the stabilization mechanism enabled by the inclusion of H_2O is unclear, but will be a topic of future investigation.

4 Conclusions

In summary, we have shown that the incorporation of controlled volumes of water into the PbI_2 precursor, similar to those expected due to inadvertent exposure of PbI_2/DMF solutions to moist air, causes significant changes in the performance of sequentially spin-coated perovskite devices. Increasing concentrations of water are observed not only to reduce overall device performance, but also to exaggerate the scan rate and directional dependent hysteresis of the devices. We propose that the addition of water to the precursor solution results in a higher concentration of mobile ions in the final perovskite film, which migrate under bias, causing JV hysteresis. Surprisingly, the inclusion of water in the perovskite film is also observed to have a stabilizing effect on long-term device performance; at best an approximately 9 % decrease in PCE was observed for a device with 1 mol% H_2O after 20 days in comparison with the a device fabricated from completely anhydrous precursors, which experienced approximately a 25 % decrease in PCE. In addition, the PCE of the best 1 % device exceeds that of the best anhydrous device after 20 days.

References

1 A. Kojima, K. Teshima, Y. Shirai and T. Miyasaka, *Journal of the American Chemical Society*, 2009, **131**, 6050–6051.

2 W. S. Yang, J. H. Noh, N. J. Jeon, Y. C. Kim, S. Ryu, J. Seo and S. I. Seok, *Science*, 2015, 1234–1237.

3 C. Wehrenfennig, G. E. Eperon, M. B. Johnston, H. J. Snaith and L. M. Herz, *Advanced Materials*, 2014, **26**, 1584–1589.

4 G. Xing, N. Mathews, S. Sun, S. S. Lim, Y. M. Lam, M. Grätzel, S. Mhaisalkar and T. C. Sum, *Science*, 2013, **342**, 344–347.

5 S. D. Stranks, G. E. Eperon, G. Grancini, C. Menelaou, M. J. Alcocer, T. Leijtens, L. M. Herz, A. Petrozza and H. J. Snaith, *Science*, 2013, **342**, 341–344.

6 V. D'Innocenzo, G. Grancini, M. J. Alcocer, A. R. S. Kandada, S. D. Stranks, M. M. Lee, G. Lanzani, H. J. Snaith and A. Petrozza, *Nature communications*, 2014, **5**, 1–6.

7 J. Xiong, B. Yang, R. Wu, C. Cao, Y. Huang, C. Liu, Z. Hu, H. Huang, Y. Gao and J. Yang, *Organic Electronics*, 2015, **24**, 106–112.

8 J. You, Z. Hong, Y. M. Yang, Q. Chen, M. Cai, T.-B. Song, C.-C. Chen, S. Lu, Y. Liu, H. Zhou *et al.*, *ACS Nano*, 2014, **8**, 1674–1680.

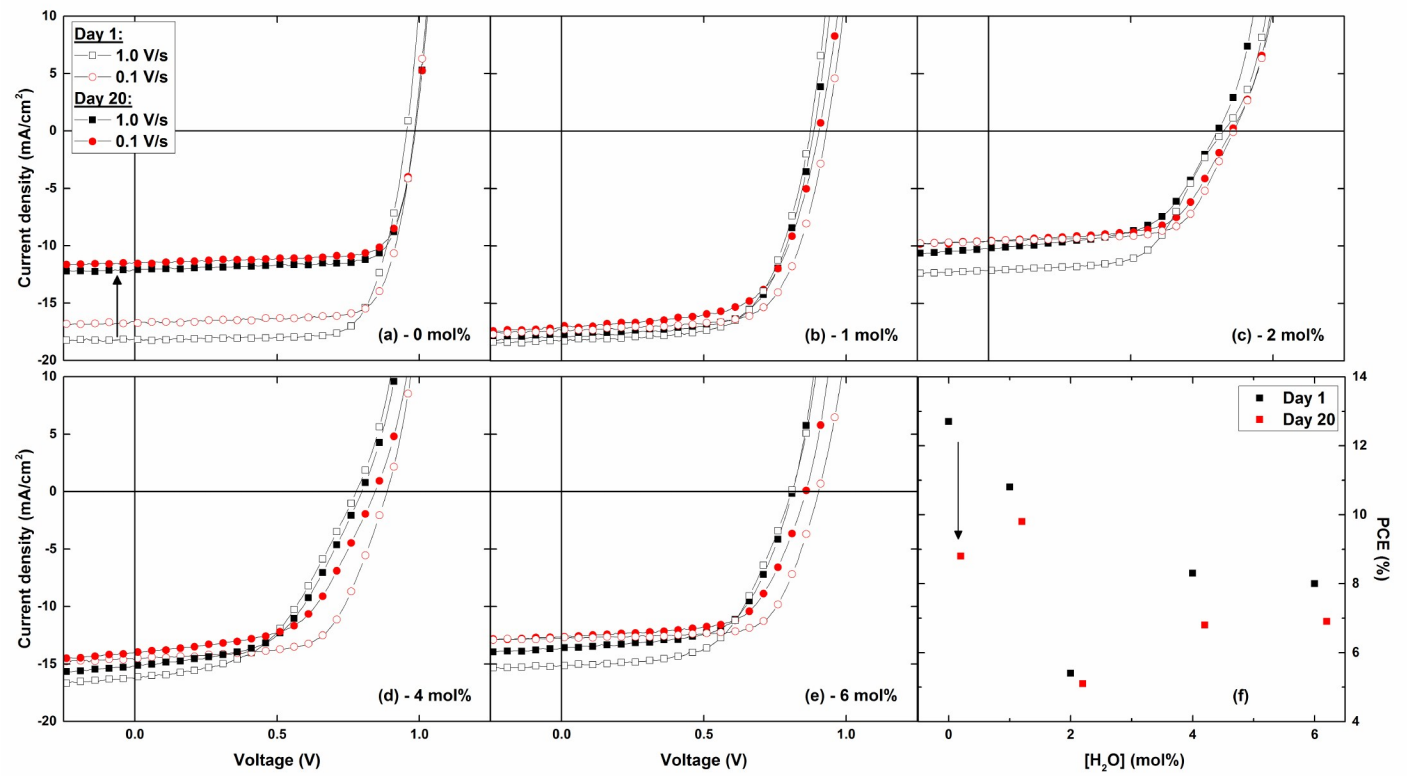

Fig. 8 JV curves for devices with varying water concentrations measured 1 day (unshaded symbols) and 20 days (shaded symbols) post-fabrication. Two scan rates are shown (1.0 V/s, black; and, 0.1 V/s, red). The performance metrics for the 0.1 V/s scans on days 1 and 20 are presented in the final panel, and summarized in Table 1.

Table 1 Comparison of device performance metrics measured before and after 20 days storage in an argon glovebox.

$[H_2O]$ (mol %)	Voc (V)		Jsc (mA/cm2)		PCE (%)		FF	
	Day 1	Day 20	Day 1	Day 20	Day 1	Day 20	Day 1	Day 20
0	0.998	0.995	16.83	11.43	12.7	8.8	0.76	0.77
1	0.949	0.916	17.19	17.11	10.8	9.8	0.66	0.63
2	0.878	0.865	9.51	9.53	5.4	5.1	0.65	0.61
4	0.894	0.845	14.64	14.09	8.3	6.8	0.63	0.57
6	0.917	0.861	12.81	12.66	8.0	6.9	0.68	0.63

9 Q. Xue, Z. Hu, J. Liu, J. Lin, C. Sun, Z. Chen, C. Duan, J. Wang, C. Liao, W. M. Lau, F. Huang, H.-L. Yip and Y. Cao, *Journal of Materials Chemistry A*, 2014, **2**, 19598–19603.

10 Z. Xiao, C. Bi, Y. Shao, Q. Dong, Q. Wang, Y. Yuan, C. Wang, Y. Gao and J. Huang, *Energy & Environmental Science*, 2014, **7**, 2619–2623.

11 O. Malinkiewicz, A. Yella, Y. H. Lee, G. M. Espallargas, M. Graetzel, M. K. Nazeeruddin and H. J. Bolink, *Nature Photonics*, 2014, **8**, 128–132.

12 J. Seo, S. Park, Y. C. Kim, N. J. Jeon, J. H. Noh, S. C. Yoon and S. I. Seok, *Energy & Environmental Science*, 2014, **7**, 2642–2646.

13 C.-H. Chiang, Z.-L. Tseng and C.-G. Wu, *Journal of Materials Chemistry A*, 2014, **2**, 15897–15903.

14 S.-G. Li, K.-J. Jiang, M.-J. Su, X.-P. Cui, J.-H. Huang, Q.-Q. Zhang, X.-Q. Zhou, L.-M. Yang and Y.-L. Song, *Journal of Materials Chemistry A*, 2015, **3**, 9092–9097.

15 K. Hwang, Y.-S. Jung, Y.-J. Heo, F. H. Scholes, S. E. Watkins, J. Subbiah, D. J. Jones, D.-Y. Kim and D. Vak, *Advanced Materials*, 2015, **27**, 1241–1247.

16 J. M. Frost, K. T. Butler, F. Brivio, C. H. Hendon, M. Van Schilfgaarde and A. Walsh, *Nano letters*, 2014, **14**, 2584–2590.

17 B. Hailegnaw, S. Kirmayer, E. Edri, G. Hodes and D. Cahen, *The Journal of Physical Chemistry Letters*, 2015, **6**, 1543–1547.

18 J. Yang, B. D. Siempelkamp, D. Liu and T. L. Kelly, *ACS Nano*, 2015, **9**, 1955–1963.

19 A. M. Leguy, Y. Hu, M. Campoy-Quiles, M. I. Alonso, O. J. Weber, P. Azarhoosh, M. Van Schilfgaarde, M. T. Weller, T. Bein, J. Nelson *et al.*, *Chemistry of Materials*, 2015, **27**, 3397–3407.

20 A. Guerrero, J. You, C. Aranda, Y. S. Kang, G. Garcia-Belmonte, H. Zhou, J. Bisquert and Y. Yang, *ACS nano*, 2015, **10**, 218–224.

21 C. Mï£iller, T. Glaser, M. Plogmeyer, M. Sendner, S. Dï£iring, A. A. Bakulin, C. Brzuska, R. Scheer, M. S. Pshenichnikov,

W. Kowalsky *et al.*, *Chemistry of Materials*, 2015, **27**, 7835–7841.

22 E. Mosconi, J. M. Azpiroz and F. De Angelis, *Chemistry of Materials*, 2015, **27**, 4885–4892.

23 J. A. Christians, P. A. Miranda Herrera and P. V. Kamat, *Journal of the American Chemical Society*, 2015, **137**, 1530–1538.

24 W. Zhou, Y. Zhao, C. Shi, H. Huang, J. Wei, R. Fu, K. Liu, D. Yu and Q. Zhao, *The Journal of Physical Chemistry C*, 2016, **120**, 4759–4765.

25 H. Zhou, Q. Chen, G. Li, S. Luo, T.-B. Song, H.-S. Duan, Z. Hong, J. You, Y. Liu and Y. Yang, *Science*, 2014, **345**, 542–546.

26 J. You, Y. M. Yang, Z. Hong, T.-B. Song, L. Meng, Y. Liu, C. Jiang, H. Zhou, W.-H. Chang, G. Li *et al.*, *Applied Physics Letters*, 2014, **105**, 183902.

27 S. Pathak, A. Sepe, A. Sadhanala, F. Deschler, A. Haghighirad, N. Sakai, K. C. Goedel, S. D. Stranks, N. Noel, M. Price *et al.*, *ACS nano*, 2015, **9**, 2311–2320.

28 G. E. Eperon, S. N. Habisreutinger, T. Leijtens, B. J. Bruijnaers, J. J. van Franeker, D. W. deQuilettes, S. Pathak, R. J. Sutton, G. Grancini, D. S. Ginger *et al.*, *ACS nano*, 2015, **9**, 9380–9393.

29 M. K. Gangishetty, R. W. Scott and T. L. Kelly, *Nanoscale*, 2016, **8**, 6300–6307.

30 C.-G. Wu, C.-H. Chiang, Z.-L. Tseng, M. K. Nazeeruddin, A. Hagfeldt and M. Grätzel, *Energy & Environmental Science*, 2015, **8**, 2725–2733.

31 N. Adhikari, A. Dubey, E. A. Gaml, B. Vaagensmith, K. M. Reza, S. A. A. Mabrouk, S. Gu, J. Zai, X. Qian and Q. Qiao, *Nanoscale*, 2016, **8**, 2693–2703.

32 B. Conings, A. Babayigit, T. Vangerven, J. D'Haen, J. Manca and H.-G. Boyen, *Journal of Materials Chemistry A*, 2015, **3**, 19123–19128.

33 X. Gong, M. Li, X.-B. Shi, H. Ma, Z.-K. Wang and L.-S. Liao, *Advanced Functional Materials*, 2015, **25**, 6671–6678.

34 G. E. Eperon, V. M. Burlakov, P. Docampo, A. Goriely and H. J. Snaith, *Advanced Functional Materials*, 2014, **24**, 151–157.

35 J.-H. Im, H.-S. Kim and N.-G. Park, *Apl Materials*, 2014, **2**, 081510.

36 P. Docampo, J. M. Ball, M. Darwich, G. E. Eperon and H. J. Snaith, *Nature communications*, 2013, **4**, 1–6.

37 Y. Hui and R. D. Webster, *Analytical chemistry*, 2011, **83**, 976–981.

38 T. Ivanova and B. Geller, *Zhurnal Fizicheskoi Khimii*, 1961, **35**, 1221–1229.

39 J. Juillard, *Pure Appl Chem*, 1977, **49**, 885–892.

40 E. Unger, E. Hoke, C. Bailie, W. Nguyen, A. Bowring, T. Heumüller, M. Christoforo and M. McGehee, *Energy & Environmental Science*, 2014, **7**, 3690–3698.

41 H. J. Snaith, A. Abate, J. M. Ball, G. E. Eperon, T. Leijtens, N. K. Noel, S. D. Stranks, J. T.-W. Wang, K. Wojciechowski and W. Zhang, *The Journal of Physical Chemistry Letters*, 2014, **5**, 1511–1515.

42 B. C. O'Regan, P. R. Barnes, X. Li, C. Law, E. Palomares and J. M. Marin-Beloqui, *Journal of the American Chemical Society*, 2015, **137**, 5087–5099.

43 W. Tress, N. Marinova, T. Moehl, S. Zakeeruddin, M. K. Nazeeruddin and M. Grätzel, *Energy & Environmental Science*, 2015, **8**, 995–1004.

44 J. H. Heo, H. J. Han, D. Kim, T. K. Ahn and S. H. Im, *Energy & Environmental Science*, 2015, **8**, 1602–1608.

45 H.-S. Kim, I.-H. Jang, N. Ahn, M. Choi, A. Guerrero, J. Bisquert and N.-G. Park, *The journal of physical chemistry letters*, 2015, **6**, 4633–4639.

46 J. Carrillo, A. Guerrero, S. Rahimnejad, O. Almora, I. Zarazua, E. Mas-Marza, J. Bisquert and G. Garcia-Belmonte, *Advanced Energy Materials*, 2016.

47 Y. Shao, Z. Xiao, C. Bi, Y. Yuan and J. Huang, *Nature communications*, 2014, **5**, 1–7.

48 J. Xu, A. Buin, A. H. Ip, W. Li, O. Voznyy, R. Comin, M. Yuan, S. Jeon, Z. Ning, J. J. McDowell *et al.*, *Nature communications*, 2015, **6**, 1–8.

49 C. Zhao, B. Chen, X. Qiao, L. Luan, K. Lu and B. Hu, *Advanced Energy Materials*, 2015, **5**, 1–6.

50 C. Eames, J. M. Frost, P. R. Barnes, B. C. O'regan, A. Walsh and M. S. Islam, *Nature communications*, 2015, **6**, 1–6.

51 J. M. Azpiroz, E. Mosconi, J. Bisquert and F. De Angelis, *Energy & Environmental Science*, 2015, **8**, 2118–2127.

52 J. Haruyama, K. Sodeyama, L. Han and Y. Tateyama, *Journal of the American Chemical Society*, 2015, **137**, 10048–10051.

53 Y. Shao, Y. Fang, T. Li, Q. Wang, Q. Dong, Y. Deng, Y. Yuan, H. Wei, M. Wang, A. Gruverman *et al.*, *Energy & Environmental Science*, 2016.

54 G. Niu, W. Li, F. Meng, L. Wang, H. Dong and Y. Qiu, *Journal of Materials Chemistry A*, 2014, **2**, 705–710.

55 B. R. Vincent, K. N. Robertson, T. S. Cameron and O. Knop, *Canadian journal of chemistry*, 1987, **65**, 1042–1046.

56 D. A. Egger, L. Kronik and A. M. Rappe, *Angewandte Chemie International Edition*, 2015, **54**, 12437–12441.

57 Q. Chen, H. Zhou, T.-B. Song, S. Luo, Z. Hong, H.-S. Duan, L. Dou, Y. Liu and Y. Yang, *Nano letters*, 2014, **14**, 4158–4163.

58 T. Supasai, N. Rujisamphan, K. Ullrich, A. Chemseddine and T. Dittrich, *Applied Physics Letters*, 2013, **103**, 183906.

59 Z. Xiao, Q. Dong, C. Bi, Y. Shao, Y. Yuan and J. Huang, *Advanced Materials*, 2014, **26**, 6503–6509.

60 K. W. Tan, D. T. Moore, M. Saliba, H. Sai, L. A. Estroff, T. Hanrath, H. J. Snaith and U. Wiesner, *ACS nano*, 2014, **8**, 4730–4739.

61 G. Grancini, V. D'Innocenzo, E. Dohner, N. Martino, A. S. Kandada, E. Mosconi, F. De Angelis, H. Karunadasa, E. Hoke and A. Petrozza, *Chemical Science*, 2015, **6**, 7305–7310.

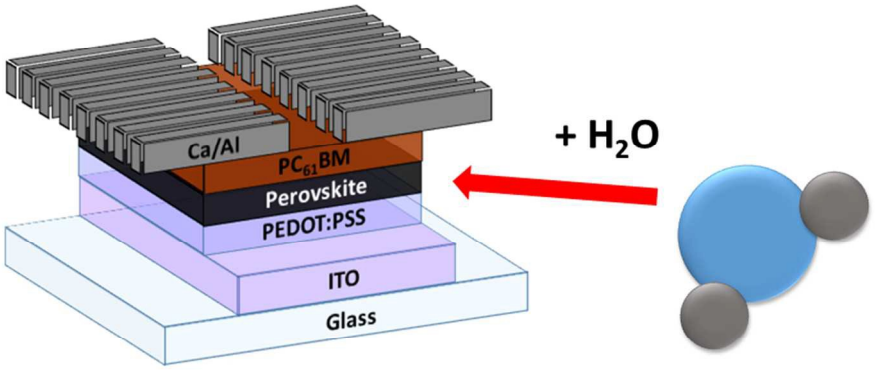

253x146mm (96 x 96 DPI)